Available online at www.sciencedirect.com

ScienceDirect

Manufacturing Letters 3 (2015) 9–13

www.elsevier.com/locate/mfglet

Research Letters

The machining temperature during Spark Assisted Chemical Engraving of glass

Jana D. Abou Ziki, Lucas A. Hof, Rolf Wüthrich *

Department of Mechanical & Industrial Engineering, Concordia University, 1455 de Maisonneuve Blvd. West, Montreal H3G 1M8, Canada

Received 26 July 2014; received in revised form 16 October 2014; accepted 30 November 2014
Available online 5 December 2014

Abstract

The temperature at which Spark Assisted Chemical Engraving (SACE) takes place is a debated question. Several models were built to predict the material removal rate, but each assumed a different machining temperature. This communication aims to give clarification about the machining temperature. It is shown that this temperature can vary depending on the drilling strategy and the machined structure geometry. This work deepens the understanding of the SACE machining process and it aims to help in future developments of models to estimate the temperature and machining rate for SACE.

Keywords: Spark Assisted Chemical Engraving; Machining temperature; Thermal-assisted etching; Glass micro-machining

1. Introduction

Spark Assisted Chemical Engraving (SACE) is one of the technologies applied for machining glass [1]. The machining process is due to the generation of electrochemical discharges through a gas film formed at the tool-electrode tip resulting in increased local temperature and high temperature etching of glass [1].

Till the present day, there are controversial opinions about the local temperature while machining. In fact, different models were built to estimate the material removal rate during machining where all assume different machining temperatures. While some postulate that machining occurs at the glass melting point, others assume that the glass is softened during the process. For example, temperatures of 870 K [2,3], 1423 K [4], 1193 K [5], above 1093 K [6] and 14,000 K [7] were used as inputs for the various models. No model currently exists that allows estimating the local temperature during SACE machining based on the applied machining conditions.

In this communication, information about the local temperature during SACE machining is presented. Results show that there is not one specific machining temperature during SACE machining. In fact, the local machining temperature varies depending on the machining strategy used and the machined structure geometry, which are influenced by local flushing. The present discussion shows that for advancing the field of SACE machining, developing heat transfer models that can predict the temperature in function of the machining conditions are crucial.

2. Experimental methods

The set-up described in [8] is used to conduct the experiments for this work. In short, the tool-electrode is fixed to the machining head (Z-motion) and the glass substrate is mounted in the processing cell which can move in the X and Y directions. To ensure that the tool bottom surface and the substrate are aligned, the tool was polished while mounted on the machining head. A polishing paper, 800

* Corresponding author. Tel.: +1 514 8482424x3150.
E-mail address: rolf.wuthrich@concordia.ca (R. Wüthrich).

http://dx.doi.org/10.1016/j.mfglet.2014.11.003

grit size, is glued to the glass work-piece. The last is moved back and forth at 100 μm/s during 10 min while the tool is pressed against it (a force less than 0.1 N is applied). The tool is rotated at 300 rpm. The resulting surface roughness is around 0.1 μm.

Experiments are done right after this procedure without disassembling the tool. The surfaces are machined using a 500 μm diameter stainless steel tool-electrode positioned at a specific distance from the glass surface. Positioning errors resulting from tool thermal expansion and tool bending are considered based on [9,10]. The surfaces are machined while the tool is held at the same position during a certain time where the voltage is switched on. Pulsed voltage was applied in order to control the tool temperature [10]. The pulses, 20 ms on-time and 1 ms off-time, were 29 V in amplitude and were applied for different durations ranging from 100 to 1000 ms. The electrolytic solution used is 50 wt% KOH. For each set of machining conditions 10 samples were machined.

3. Discussion

SACE machining is known to be caused by etching at high localised temperatures [11–13]. The discharges generated locally from the tool sharp edges through a gas film formed round the tool tip, cause high temperature beneath the tool electrode. Therefore, the rate of etching by OH radicals supplied from the electrolytic solution increases which causes local glass machining by breaking the Si–O–Si bonds (Fig. 1a). Physical impact of discharges with the surface also contribute to machining. In fact, their impact causes glass sublimation where micro-craters are formed. Fig. 1b is an example of a micro-crater formed on the surface around which a glass layer is reformed. However, this case could be very rarely observed when examining machined structures. Therefore, the main effect contributing to glass machining is thermal-assisted etching.

In principle, etching can happen even at ambient temperature but the etch rate would be low and not localised. In fact, etching must be localised in order to machine structures on the substrate. For etching to occur the electrolyte must be in liquid state, either in aqueous or molten salt form. When the electrolyte solidifies, machining is hindered. This occurs whenever the local temperature exceeds the electrolyte vaporisation temperature (between 100 and 200 °C for NaOH and KOH depending the concentration of the aqueous solution) but remains below the electrolyte salt melting point (318 °C for NaOH and 406 °C for KOH [14,15]).

The local glass surface temperature depends on the drilling strategy used and on the machined geometry. In this work, three cases relevant for SACE machining are discussed (Fig. 2). When the tool is in contact with the glass surface, such as in gravity-feed drilling, the machining temperature T_M will be similar to that of the tool T_{tool} which can reach 500–600 °C [10] (Fig. 2a). The model developed by Jalali et al. [3] for gravity-feed drilling reproduces well the experimental drilling speeds using this temperature as an input. Similar agreement is found in the model of Jiang et al. [2] when using the same machining temperature for their calculations.

In case the tool is fed at a rate lower than the machining rate, a gap grows between the tool and the glass surface. As the gap grows, the temperature of the work-piece surface decreases until reaching the electrolyte salt melting temperature $T_{melting}$ (Fig. 2b). The validity of this mechanism was demonstrated recently by Abou Ziki et al. [9,16] while studying the gap between tool and work-piece in case of glass micro-drilling.

For shallow structures or for 2D machined surfaces, flushing the machined material and bubbles from the machining zone will not be a problem. Hence, the electrolyte cannot reach a high enough temperature to become a molten salt due to the continuous flushing. The electrolyte remains in aqueous form and has a maximal temperature around its vaporisation temperature $T_{vaporisation}$ as depicted in (Fig. 2c). This aspect was so far never verified experimentally in the literature.

Fig. 3 shows the typical machined surfaces for various machining durations and for a zero tool-substrate gap. Results show that a ring of outer diameter similar to that of the tool is formed for the smallest machining duration. For higher machining durations, the ring grows radially in the inward direction towards the center of the surface beneath the tool. The ring inner diameter, as depicted on Fig. 3, decreases until the complete surface beneath the tool is machined. For this particular example, this occurs starting from a machining duration of about 800 ms. The machining temperature can be estimated by matching the ring growth (inner diameter) over time with the temperature isotherm calculated by a semi-infinite transient thermal model built in ANSYS software [9]. The heat source is considered a ring of 10 μm width and having the same outer diameter as that of the tool. Temperature isotherms are calculated using the transient model by applying the initial and boundary conditions below (Eqs. (1)–(4)), assuming that the material is homogeneous and isotropic and that the applied thermal load distribution is uniform. The effect of local flow (natural convection and radiation) is neglected. The initial condition is:

$$T(x,y,z,t) = T_0 \tag{1}$$

where $T(x,y,z,t)$ is the work-piece temperature field and T_0 is its initial temperature.

The boundary conditions on the edges of the semi-infinite simulated volume are:

$$\frac{\partial T}{\partial n} = 0 \tag{2}$$

where n is the normal to the plane at which heat propagates. On the heat source ring, the boundary condition is:

$$\lambda \frac{\partial T}{\partial n} = -\dot{q} \tag{3}$$

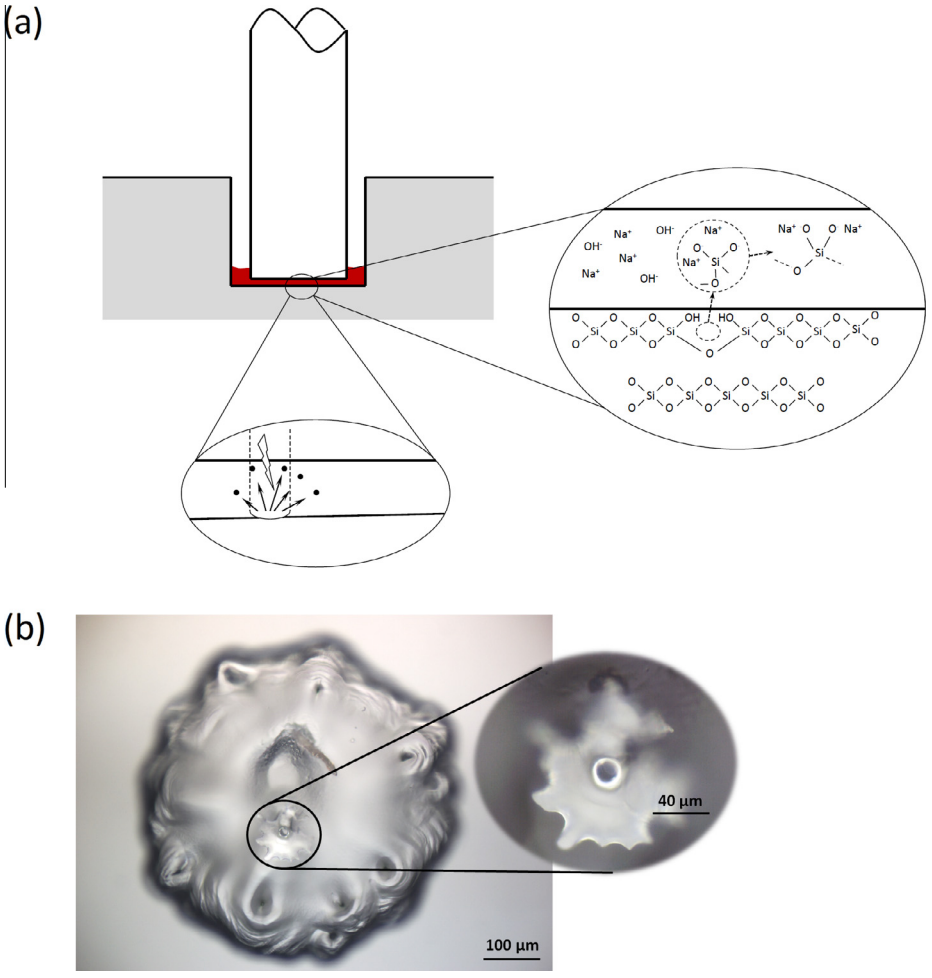

Figure 1. (a) Schematic of the SACE machining mechanism. Machining occurs due to the chemical attack of glass by OH radicals that break the Si–O–Si glass bonds, and by physical bombardment of the glass surface by discharges. (b) A micro-crater formed on the surface due to discharge impact. The crater is surrounded by a layer of splashed glass.

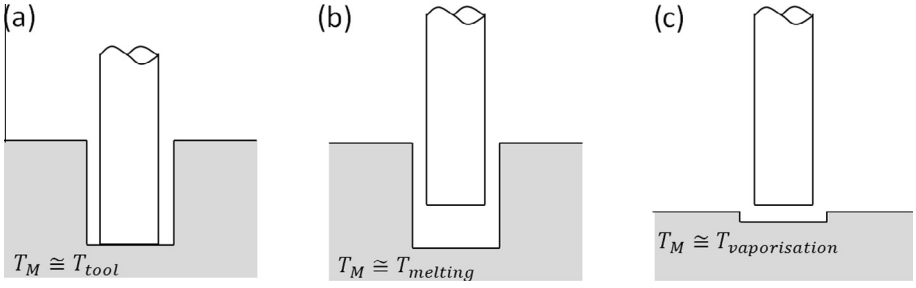

Figure 2. Schematic of three cases relevant to SACE machining: (a) For deep holes where tool–glass contact occurs frequently, the machining temperature is similar to that of the tool ($T_M = T_{tool}$), (b) When a machining gap is formed during drilling, the machining temperature is similar to the melting temperature of the electrolyte salt ($T_M = T_{melting}$), and (c) For shallow structures the machining temperature is similar to the electrolyte vaporisation temperature ($T_M = T_{vaporisation}$).

where $\dot{q}$ is the heat flux generated by the discharges during the SACE process and λ is the glass substrate thermal conductivity.

The heat flux is considered to be locate on the glass surface and is calculated as follows:

$$\dot{q} = \frac{U \cdot \bar{I}}{A} \tag{4}$$

where U is the voltage, $\bar{I}$ is the mean current (0.01 A for 29 V based on [10]) and A is the surface area of the heat source which is a ring having the same tool diameter and 10 µm wide. Detailed description of the finite-element model can be found in [9].

Fig. 4 shows the size of the machined rings for three temperature isotherms (177, 185 and 195 °C) for the

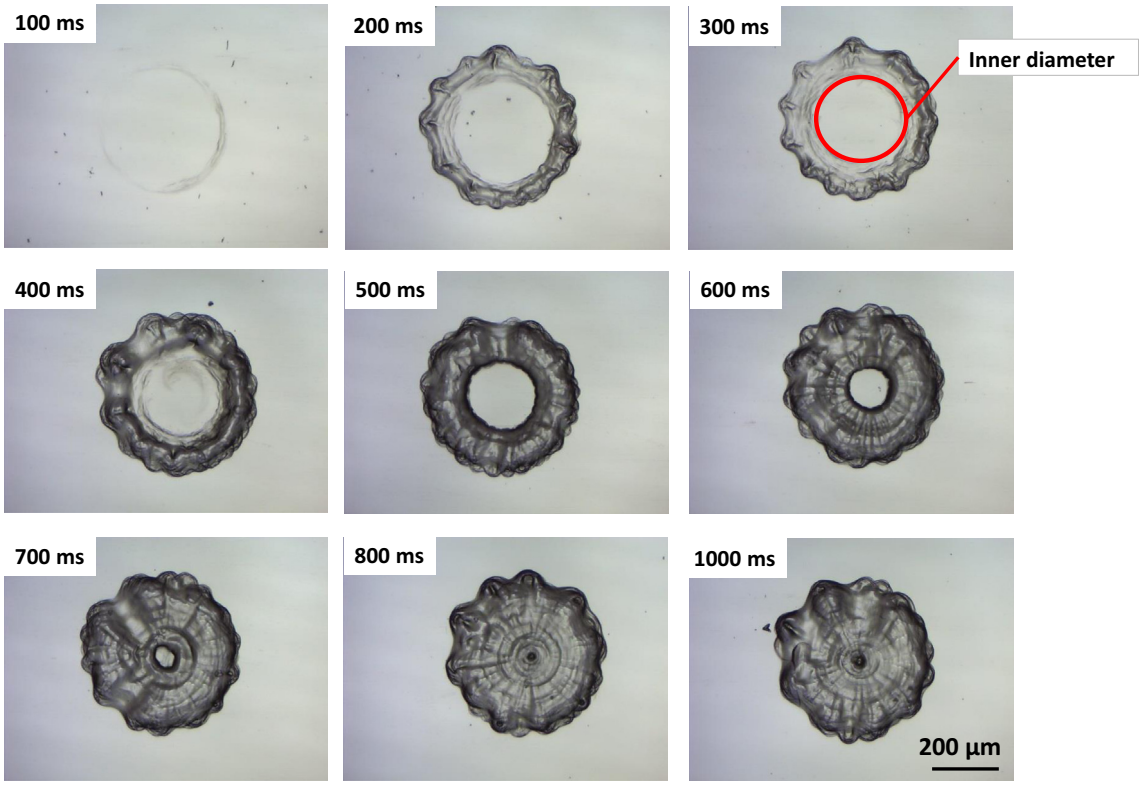

Figure 3. Shallow structures machined in 50 wt% KOH while applying 29 V pulsed voltage (20 ms on-time and 1 ms off-time) using a 500 µm diameter stainless steel tool. The voltage is applied during different durations ranging from 100 to 1000 ms. The structures' inner diameter is reduced as they evolve from rings into a complete machined disk for increased machining duration.

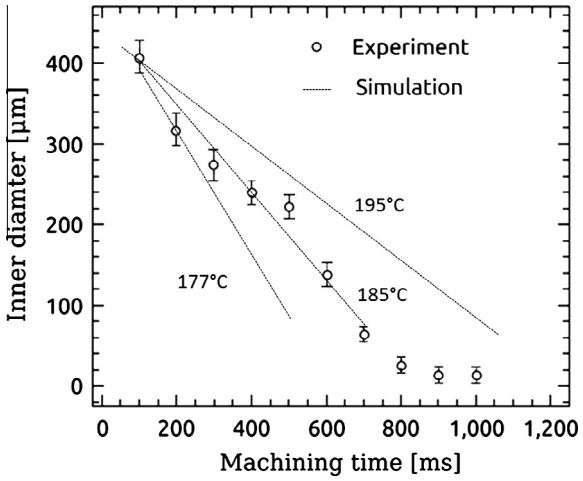

Figure 4. Machined and calculated inner diameters (based on a heat transfer model) for shallow structures in function of machining time. The machined diameters match with the calculated ones for a temperature isotherm of 185 °C (around the electrolyte vaporisation temperature). This corresponds to the machining temperature for these applied conditions.

different applied machining durations. Results show that the size of the machined rings best corresponds with that of the 185 °C isotherm, which is around the vaporisation temperature of the electrolytic solution (185 °C is the boiling point of a 62 wt% KOH solution).

These results show the necessity of building general heat transfer models for the SACE machining process having the machining temperature as an output contrary to the recent SACE models which consider this temperature as an input. This is a challenging task knowing the complexity of the multi-phase flow.

4. Conclusion

In this letter, the machining temperature during SACE process is discussed. SACE machining is caused mainly by etching. Therefore, machining can occur at different temperatures, but only those that would allow the electrolyte to stay either aqueous or molten. Results showed that the local temperature depends on the machining configuration and the machined surface geometry which affect local flushing. For shallow structures, electrolyte is aqueous where its temperature is around its vaporisation temperature. However, for deep structures, the temperature is higher and can reach that of the tool in case of tool–glass contact. Therefore, electrolyte appears in molten form.

The present results show the need to build transient heat transfer models to estimate the machining temperature for applied machining conditions rather than using the temperature as an input. This is a challenging task as these models must consider the complex multiphase local flow.

Acknowledgments

This work was supported by the Natural Sciences and Engineering Research Council of Canada (NSERC). J.D.A.Z. would like to thank the Ministère de l'Education, du Loisir et du Sport du Quebec (MELS) for the bourse d'excellence pour étudiants étrangers (V1) and Posalux SA for the Posalux Excellence Scholarship.

References

[1] Wüthrich R. Micromachining using electrochemical discharge phenomenon: fundamentals and applications of spark assisted chemical engraving. Norwich, NY, USA: William Andrew; 2009.
[2] Jiang B, Lan S, Ni J, Zhang Z. Experimental investigation of spark generation in electrochemical discharge machining of non-conducting materials. J Mater Process Technol 2014;214:892–8.
[3] Jalali M, Maillard P, Wüthrich R. Toward a better understanding of glass gravity-feed micro-hole drilling with electrochemical discharges. J Micromech Microeng 2009;19(4):045001.
[4] Panda M, Yadava V. Finite element prediction of material removal rate due to traveling wire electrochemical spark machining. Int J Adv Manuf Technol 2009;45:506–20.
[5] Fascio V, Wüthrich R, Bleuler H. Spark assisted chemical engraving in the light of electrochemistry. Electrochim Acta 2004;49:3997–4003.
[6] Jain V, Dixit P, Pandey P. On the analysis of the electrochemical spark machining process. Int J Mach Tool Manuf 1999;39:165–86.
[7] Bhondwe K, Yadava V, Kathiresan G. Finite element prediction of material removal rate due to electro-chemical spark machining. Int J Mach Tool Manuf 2006;46:1699–706.
[8] Abou Ziki JD, Wüthrich R. Forces exerted on the tool-electrode during constant-feed glass micro-drilling by spark assisted chemical engraving. Int J Mach Tool Manuf 2013;73:47–54.
[9] Abou Ziki J.D., 2014. Spark assisted chemical engraving: a novel approach for quantifying the machining zone's parameters using drilling forces (Ph.D. thesis). Concordia University, Canada.
[10] Abou Ziki JD, Wüthrich R. Tool wear and tool thermal expansion during micro-machining by spark assisted chemical engraving. Int J Adv Manuf Technol 2012;61:481–6.
[11] Tokura H, Kondoh I, Yoshikswa M. Ceramic material processing by electrical discharge in electrolyte. J Mater Sci 1989;24:991–8.
[12] Yang C, Ho S, Yan B. Micro hole machining of borosilicate glass through electrochemical discharge machining (ECDM). Key Eng Mater 2001;196:149–66.
[13] Jain V, Adhikary S. On the mechanism of material removal in electrochemical spark machining of quartz under different polarity conditions. J Mater Process Technol 2008;200:460–70.
[14] OxyChem, 2000. Oxychem caustic potash handbook. Available at: <http://www.oxychile.cl/ingles/>.
[15] Oxychem caustic soda handbook, 2009. <http://www.cheresources.com/invision/uploads/images/technicaldatabase/oxycaustic.pdf>.
[16] Abou Ziki JD, Wüthrich R. The machining gap during constant velocity-feed glass micro-drilling by spark assisted chemical engraving (accepted for publication).